

# Lipid exchange in crystal-confined Fatty Acid Binding Proteins: X-ray evidence and Molecular Dynamics explanation

H. Ariel Alvarez<sup>1</sup>, Alexandra Cousido-Siah<sup>2</sup>, Yanis R. Espinosa<sup>1</sup>, alberto podjarny<sup>2</sup>, C. Manuel Carlevaro<sup>1</sup>, and Eduardo Howard<sup>1</sup>

<sup>1</sup>Instituto de Fisica de Liquidos y Sistemas Biologicos

<sup>2</sup>Institut de Genetique et de Biologie Moleculaire et Cellulaire

March 30, 2023

# Lipid exchange in crystal-confined Fatty Acid Binding Proteins: X-ray evidence and Molecular Dynamics explanation

H. Ariel Alvarez PhD<sup>1,2,3\*</sup> | Alexandra Cousido-Siah PhD<sup>4\*</sup>  
| Yanis R. Espinosa PhD<sup>1,5</sup> | Alberto Podjarny PhD<sup>4</sup> |  
Manuel Carlevaro PhD<sup>1,6†</sup> | Eduardo Howard PhD<sup>1,7†</sup>

<sup>1</sup>Instituto de Física de Líquidos y Sistemas Biológicos (UNLP-CONICET), La Plata, Buenos Aires, Argentina.

<sup>2</sup>Departamento de Ciencias Biológicas, Facultad de Ciencias Exactas, Universidad Nacional de La Plata, La Plata, Buenos Aires, Argentina.

<sup>3</sup>Instituto de Ciencias de la Salud, Universidad Nacional Arturo Jauretche, Florencio Varela, Buenos Aires, Argentina.

<sup>4</sup>Institut de Genétique et de Biologie Moléculaire et Cellulaire, 1 Rue Laurent Fries, Illkirch-Graffenstaden, France.

<sup>5</sup>Universidad Francisco de Paula Santander, Facultad de Ciencias Agrarias y del Ambiente, Departamento de Ciencias del Medio Ambiente, Cúcuta, Colombia.

<sup>6</sup>Facultad Regional La Plata, Universidad Tecnológica Nacional, Berisso, Buenos Aires, Argentina.

<sup>7</sup>Facultad Regional Tierra del Fuego, Universidad Tecnológica Nacional, Ushuaia, Tierra del Fuego, Argentina.

## Correspondence

Email:

manuel@iflysisib.unlp.edu.ar, howard@iflysisib.unlp.edu.ar

## Funding information

Consejo Nacional de Investigaciones Científicas y Técnicas (CONICET) Grant Number: PIP 11220210100884CO

Fatty Acid Binding Proteins (FABPs) are responsible for the long-chain fatty acids transport inside the cell. But despite the years since their structure is known and the many studies published, there is no definitive answer about the stages of the lipid entry-exit mechanism. Their structure forms a  $\beta$ -barrel of 10 anti-parallel strands with a cap in a helix-turn-helix motif, and there is some consensus on the role of the so-called portal region, involving the second  $\alpha$ -helix from the cap ( $\alpha 2$ ),  $\beta C$ - $\beta D$  and  $\beta E$ - $\beta F$  turns in fatty acids exchange. To test the idea of a lid that opens, we performed a soaking experiment on an h-FABP crystal in which the cap is part of the packing contacts, and its movement is strongly restricted. Even in these conditions, we observed the replacement of palmitic acid by 2-Bromohexadecanoic acid (Br-palmitic acid). Our MD simulations reveal a two-step lipid entry process: i.- The travel of the lipid head through the cavity in the order of tens of nanoseconds, and ii.- The

---

**Abbreviations:** FA, fatty acid; hFABP, heart Fatty Acid Binding Protein; LBPs, intracellular Lipid Binding Protein; MD, Molecular Dynamics; COM, Center of Mass.

\* Equally contributing authors.

† Corresponding authors.

accommodation of its hydrophobic tail in hundreds to thousands of nanoseconds. We observed this even in the cases in which the fatty acids enter the cavity by their tail. During this process, the fatty acids do not follow a single trajectory, but multiple ones through which they get into the protein cavity. Thanks to the complementary views between experiment and simulation, we can give an approach to a mechanistic view of the exchange process.

#### KEYWORDS

Fatty Acid Binding Proteins, Crystal Molecular Dynamics Simulations, X-Ray Diffraction, Lipids Interchange, Lipid Trafficking

## 1 | INTRODUCTION

Fatty Acid Binding Proteins (FABPs) are part of the intracellular-lipid-binding proteins (iLBPs) and are responsible for the transport of long-chain fatty acids through different compartments inside the cell. This family of proteins has a relatively low sequence identity but shares a characteristic structure composed of a  $\beta$ -barrel of 10 antiparallel strands ( $\beta A$  to  $\beta J$ ), and a cap with a helix–turn–helix motif ( $\alpha 1$  and  $\alpha 2$ ), surrounding an inner cavity that accommodates fatty acids (FAs) [1, 2, 3, 4].

Due to the relevant role of this family in lipid metabolism and transport, they have been associated with various pathologies such as obesity, chronic inflammation, heart failure or cancer [5, 6, 7, 8]. They are the object of intense investigation, and hundreds of structures have been reported both in crystals and in solution. But almost all of them are in a conformation that seems to obstruct the input/output of the lipid that they transport.

Experimental and computational studies have been carried out trying to understand the conformational changes necessary to allow lipid entry and exit. No experimental result shows the lipid during the mentioned input/output process. Even when there is a consensus on the role of the so-called portal region, involving the second  $\alpha$ -helix ( $\alpha 2$ ),  $\beta C$ – $\beta D$  and  $\beta E$ – $\beta F$  turns, in fatty acid exchange, some authors have proposed other possible pathways. For example, computational evidence [9, 10, 11] supports an alternative portal in the N-terminal region or the space between disjointing  $\beta D$ – $\beta E$  strands.

In recent years, a series of experiments have tested different portal hypotheses to understand the lipid pathway, and to what extent protein fluctuations can be constrained without cancelling the possibility of lipid entry [12, 13]. In the same spirit, we want to test the possibility of lipid exchange even when the proteins are 'trapped' in a crystal, and only fluctuations compatible with crystal packing are possible.

This could be achieved using the crystal obtained with symmetry  $P2_1 2_1 2_1$ , which especially restricts the mobility of the helix–turn–helix motif but exposes other regions of the portal to the crystal interior channels (Figure 1 and Supplemental Video 1). These channels allow fatty acids to migrate through them without significantly perturbing the crystal.

Thus, we designed an experiment where we soaked an h-FABP crystal in a solution containing Br-palmitic acid. We have chosen this molecule because the electronic density of the Bromine atom would unequivocally evidence the

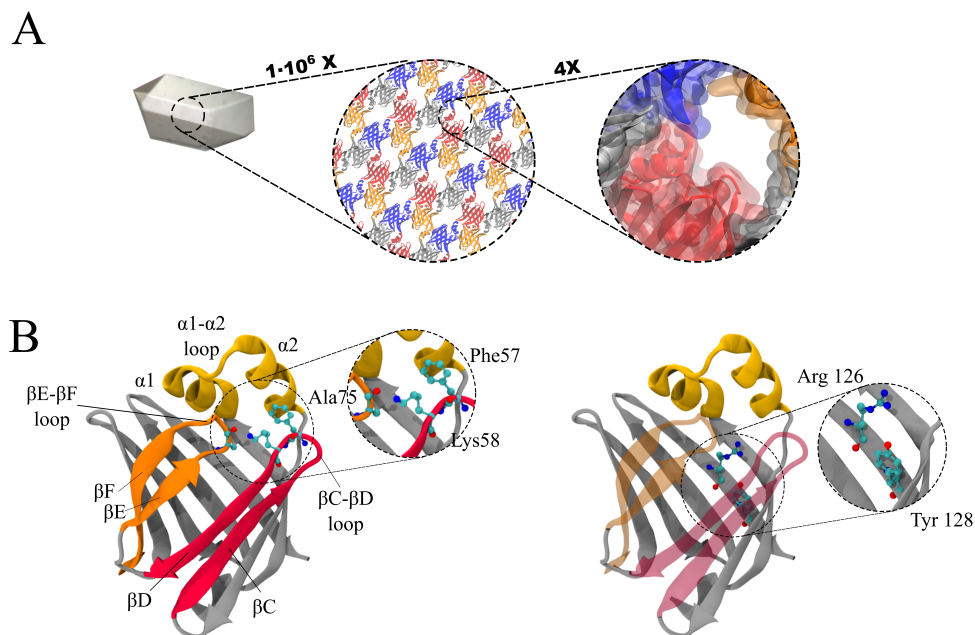


**FIGURE 1** Description of the crystal and structure of h-FABP. **A.-** Picture of the crystal (arbitrary orientation) and representations of it at different zoom scales. In the last zoom-in the representation shows that the movement of the protein's  $\alpha 1$ -turn- $\alpha 2$  cap is blocked by crystal packing. **B.-** Structure of h-FABP in new cartoon representation.  $\beta C$  strand,  $\beta D$  strand and  $\beta C$ - $\beta D$  turn are colored in red,  $\beta E$  strand,  $\beta F$  strand and  $\beta E$ - $\beta F$  turn are colored in orange, and the helix-turn-helix motif formed by  $\alpha 1$  and  $\alpha 2$  helices is colored in yellow. The relevant amino-acids for this study are depicted in a CPK representation (*i.e.*, Phe57, Lys58, Ala75, Arg126 and Tyr128).

entry (replacement) of the fatty acid. But, as in any structure obtained by X-ray or Neutron Diffraction, the result will be the spatial and temporal average of millions of proteins and, although it could give unequivocal evidence of the exchange (Figure 2), it will not be possible to obtain a description of the input/output process, even if a subatomic resolution is reached. To complement the crystallographic vision of the fatty acid interchange process at the atomic level for each individual protein, we performed Molecular Dynamics (MD) simulations. In a previous work, we have shown the feasibility of simulating an h-FABP crystal with this technique [14]. Here we combine the use of crystals as the environment to carry out the experiment, the structure solved at a very high resolution, and the numerical simulation by MD to provide insight to a seemingly simple question that has been open for many years without a conclusive answer.

## 2 | MATERIALS AND METHODS

### 2.1 | Experimental Methods

#### 2.1.1 | Enzyme purification

h-FABP was recombinantly expressed and purified based on the procedure described previously [15, 16]. Briefly, *E. coli* BL21(DE3) strain (Novagen), transformed with the pJexpress411 plasmid containing the synthetic cDNA coding for h-FABP, was grown in LB medium at 37 °C. Protein expression was induced by the addition of 1 mM isopropyl-1-thio- $\beta$ -D-galactopyranoside (IPTG, Euromedex) after 3 hours of incubation. h-FABP was purified using 25 ml of Capto Q resin (GE Healthcare). The protein was eluted by 150 mM NaCl, 25 mM Tris-HCl pH 8.0. Then, h-FABP was purified in a superdex 75 26/60 gel filtration column, in 20 mM Tris pH 7.5, 50 mM NaCl. The obtained protein may carry U-shaped FAs with 10–18 carbon atom tails [17], but the most described in the PDB structures is C18 as, for example, in PDB-IDs 1HMR, 1HMS, 1HMT [18] or 5CE4 [19].

#### 2.1.2 | Crystallization, soaking and data collection

Crystals of h-FABP were obtained by the hanging-drop vapor diffusion method at 20 °C. The protein solution was concentrated at 20 mg/ml in 20 mM Tris pH 7.5, 50 mM NaCl, and mixed with an equal volume of precipitating solution containing 20 mM Tris pH 7.5, 20–25% polyethylene glycol (PEG) 4000. Crystals obtained in these conditions belong to the  $P2_12_12_1$  space group.

For the lipid exchange experiment, we added an ethanol solution of Br-palmitic acid (Sigma) to the mother liquor described above, until a final concentration of 12 mM was reached (6% of ethanol). The crystals were soaked in this solution for 7 days at 20 °C. After soaking, the crystals were immersed in a cryo-protecting solution containing 36% PEG 4000 and 5% ethylene glycol, and cryo-cooled in liquid nitrogen. X-ray data were collected on X06DA beamline at the Swiss Light Source synchrotron (SLS, Switzerland) at 0.97 Å resolution, and processed with HKL2000 [20].

Diffraction data were deposited in Protein Data Bank (PDB ID 8GEW). Table ?? shows Data Collection and Diffraction Statistics.

### 2.2 | Computational Methods

We generated the initial coordinates for our crystal model starting from the structure collected previously and already deposited in the PDB ID 5CE4 [19], an X-ray/neutron diffraction structure collected at room temperature. Using PyMOL [21] (*symexp* command) we applied the symmetry operations of the  $P2_12_12_1$  space group to the protein and all structural water molecules identified (crystallographic waters). The values for the unit cell dimensions were  $a = 3.4588$  nm,  $b = 5.5307$  nm,  $c = 7.1185$  nm. Considering that the length of the  $X$  axis is close to the cut-off used during the simulation (*i.e.*, 1.4 nm), we doubled the cell in this direction to avoid self-influence across periodic boundary conditions, and in this way the initial box dimensions were  $L_X = 2a = 6.9176$  nm,  $L_Y = b = 5.5307$  nm,  $L_Z = c = 7.1185$  nm (see Supplemental Video 2). Hence, the simulation box contained eight h-FABP molecules (four from each unit cell), a fatty acid per protein, 3629 TIP4P/2005 water molecules [22], and 191 ethanol molecules [23, 24]. We chose to use four palmitic acids and four oleic acids for the fatty acids since oleic acid is the most frequently reported one and because we conducted the soaking experiment using a derivative of palmitic acid.

The effective pH was assumed to be 7.5, same as in the crystallization buffer. The protonation status of individual Asp, Glu, Lys, Arg, and His residues was obtained by PROPKA [25], leading to a charge of  $-1$  per h-FABP molecule.

Thus, the net charge of each h-FABP – FA complex was  $-2$ , so sixteen  $\text{Na}^+$  counterions were added to neutralize the total charge of the system. The system was simulated using the all-atom Amber ff99SB force field [26] for protein parameters and GAFF2 force field via ACPYPE [27, 28] for palmitic and oleic acid (see Supplementary Material for the topology of the FAs). The energy minimization and equilibration processes were as described in our previous work [14] following a strategy that is oriented to preserve the dimensions of the unit cell and the structure of the protein and the lipid. To achieve this goal, the temperature was slowly raised, first allowing the solvent to equilibrate around the crystallographic structure of the protein, and then progressively releasing the movement of proteins and lipids. Also, the number of solvent molecules was selected after trial and error tests so that the volume of the system at constant pressure remains similar to the experimental one. The 5CE4 structure includes several water molecules that are visible by crystallography that were kept at the time of preparing the initial coordinates.

Five replica simulations of  $1 \mu\text{s}$  each were performed with an initial condition in which the fatty acids were randomly located in the channels of the crystal outside the proteins, and was restricted during the equilibration process. Also a control system was simulated for the same time extension with all the FAs in the protein interior. Simulations were run using the GROMACS 2018 biomolecular simulation package [29] with a 2 fs integration time step, at a temperature of 293 K and a pressure of 1 bar (NpT ensemble) by means of the Velocity Rescale thermostat [30] and Parrinello-Rahman barostat [31], respectively, during equilibration and production. Protein and non-protein groups were coupled separately to the heat bath with a relaxation time of 0.1 ps. The pressure was coupled to the barostat with a relaxation time of 2.0 ps and a compressibility of  $4.5 \cdot 10^{-5} \text{ bar}^{-1}$ . Simulations were performed with 1  $\text{C}\alpha$  atom restraint per protein. The  $\text{C}\alpha$  atom selected to restrain is the one corresponding to residue Ile114 (8 atoms over a total of 32584). This residue has a low isotropic B-factor, almost symmetric anisotropic B-factors and is far from the residues we considered in our analysis. The bond lengths were constrained using the LINCS algorithm [32] while electrostatic interactions were computed using the Particle Mesh Ewald method [33]. A cut-off of 1.4 nm was applied both for the van der Waals and Coulomb interactions with a Verlet cut-off scheme. All calculations were carried out on a Linux server Intel Core i7-6700 3.40 GHz eight Core Processor with an NVIDIA GeForce GTX 1080 GPU.

## 3 | RESULTS

### 3.1 | Experimental results

As FABPs are responsible for fatty acid trafficking inside the cell, FA interchange is an essential activity in this family of proteins. To prove if this interchange is also possible in a confined environment such as a protein crystal, we soaked the h-FABP crystal in a Br-palmitic acid solution, as described in Materials and Methods. After soaking, X-ray data were collected at 0.97 Å resolution and the structure was solved by molecular replacement (Table ??). The structure reveals the presence of Br-palmitic acid inside the cavity, using the heavy bromine atom (Br) as a marker. Our results show unambiguously that the replacement process has taken place inside the crystal. The C-Br distances (1.97 Å) correspond to an expected covalent bond (1.94 Å), evidencing that it is the whole ligand that is replaced and the electron density does not correspond to a bromine ion alone resulting from radiation damage (Figure 2). Lipid exchange during the soaking process involves the diffusion of Br-palmitic acid through the crystal channels, the release into the channel of the originally bound fatty acid (FA), and the entry of the new ligand into the protein cavity. The crystal quality of the new structure PDB 8GEW in terms of resolution and unit cell size was little affected after soaking, and they are similar (within the experimental error) to the multiple structures deposited in the PDB for this protein. Comparison of the Atomic Displacement Parameters (ADP or B-factors) of our structure with the B-factor of the structures solved by others (PDB entries 4TKJ, 4TKB, 4TKH and 4TKZ) [17], at the same data collection temperature

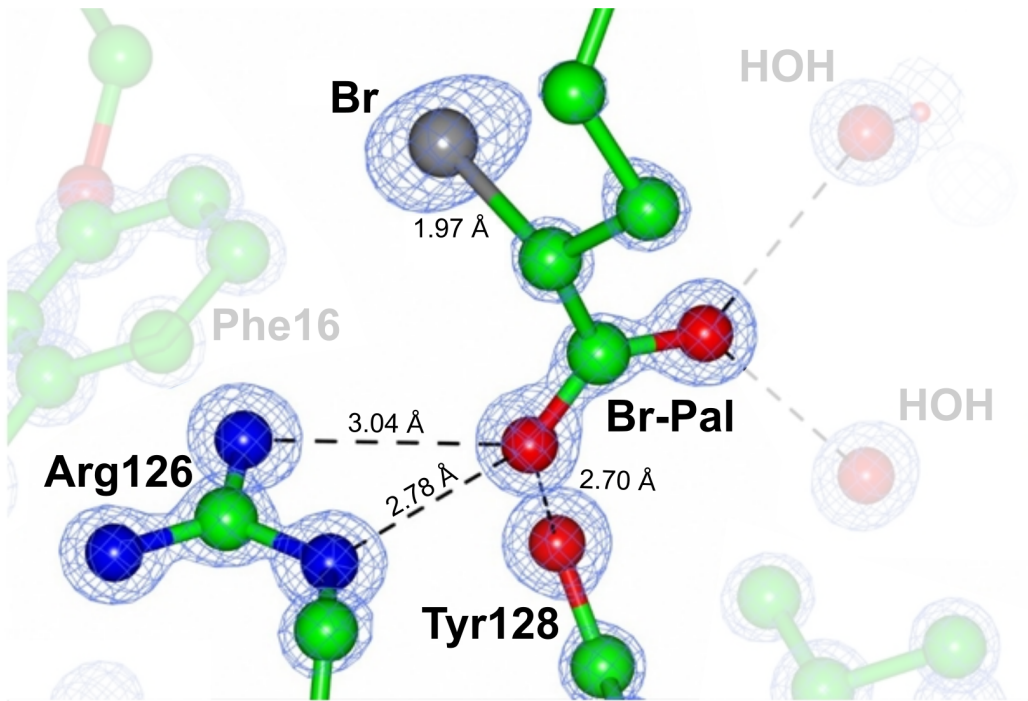


**FIGURE 2** Evidence of lipid exchange inside the crystal. 2Fo-Fc electron-density map contoured at  $4\sigma$ . Dashed lines correspond to Hydrogen bonds. The indicated Br-C distance (1.97 Å) ratifies that the Bromine atom is covalently bonded to the palmitic molecule. PDB ID 8GEW.

and comparable resolution shows a very similar distribution of values as a function of residue number (Figure S1). In particular, the sites proposed to be mobile during FA exchange have similar B-factor values in all of the compared structures.

Our crystallographic results show the final state of the interchange process, and we performed Molecular Dynamics simulations to obtain a plausible atomic description of the FA's path to achieving this final position.

### 3.2 | Molecular Dynamics results

Once the simulated crystal was equilibrated, we performed five simulation replicas of 1  $\mu$ s each, with eight FAs in the crystal channels (outside the proteins). We also performed a control simulation of 1  $\mu$ s, with the FAs in the protein interior. Additionally, we performed another simulation of 3.5  $\mu$ s with eight FAs in the protein cavity and eight in the crystal channels (Data not shown). We did not observe in any of these simulations the output of a complete FA.

To study the protein stability in the simulated crystals, we analyzed the Root Mean Square Deviation (RMSD) of the atomic coordinates of the protein backbone for all the crystal replicas in which we observed the FA entrance and for the control one. As can be seen in Figure S2, the simulations (*i.e.*, the five replicas and control) show very low values of RMSD (under 0.15 nm). We also analyzed the Atomic Displacement Parameters (ADP or B-Factors) of the atomic coordinates for the  $C\alpha$  atoms of each amino acid in the protein crystals both for the five replicas and for the

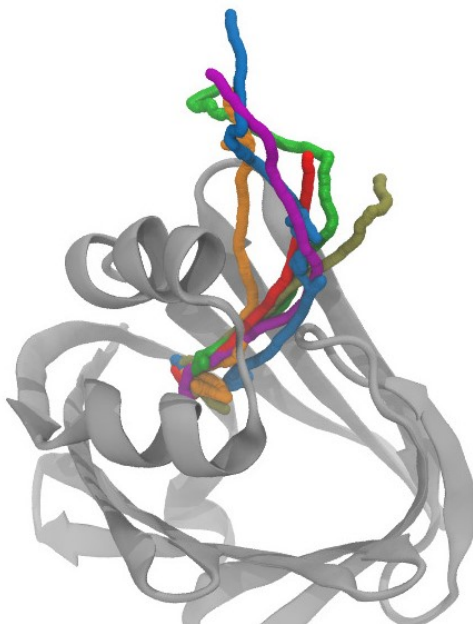


**FIGURE 3** Fatty acids enter by different pathways into the h-FABP interior. Trajectories of carboxylic carbons (C1) in the FA head entering the protein cavity for each case. Case 1 in orange, Case 2 in green, Case 3 in red, Case 4 in purple, Case 5 in olive and Case 6 in light-blue.

control simulation (see Supp. Fig. S3-A).

During the five replica simulations, we observed six FA entrance events: In cases 1 to 4 the entrance starts by the FA head and in cases 5 and 6 it starts from the FA tail. In Figure 3, we show the paths followed by carboxylic carbons (C1) from the FA head of each fatty acid in these events (as an example of how this representation was generated, see also Supplemental Video 3). To show how abrupt is the entrance event, we defined a reaction coordinate as the distance of the C1 atom of the fatty acids to its crystallographic position in 5CE4 structure and study it as a function of time (Figure 4). For clarity, the time was normalized as  $Normalized\ Time = t - t_0$ , being  $t$  the simulation time and  $t_0$  equal to the entering time in each case (time in which the reaction coordinate has a value of 1 nm, i.e., 123.05 ns, 165.45 ns, 47.65 ns, 115.55, 107.0 and 564.5 ns, for Cases 1 to 6, respectively).

The Supplemental Video 4 shows the six entrance cases. For the first 4 cases, the entrance of the FA in the protein interior involves the interaction of the FA tail with residues Ala28, Thr29, Gln31, Val32, Met35 and Thr36 from  $\alpha 2$  helix of the protein and the later entrance of the FA head into the cavity (see Figure 5). A special situation occurs in cases 5 and 6, where lipids get into the cavity through their tail. During our simulations, we have seen several cases where the tail is lodged in the cavity and the polar head moves out of the protein without reaching a stable position. But in these two cases we have observed that, after some time, the polar head manages to reach residues Arg126 and Tyr128, where it finally stabilizes.

In the first four cases, once the FA tail interacts with  $\alpha 2$  helix in the entrance path, the FA head forms hydrogen bonds with Lys58 as a previous step to the entrance (Figure 6). Then the FA head rapidly reaches its final position in the protein interior as the FA tail explores multiple conformations. The difference for cases 5 and 6 is that the hydrogen bonds with Lys58 are formed once the tail is in the cavity. During this process, neither the helix-turn-helix

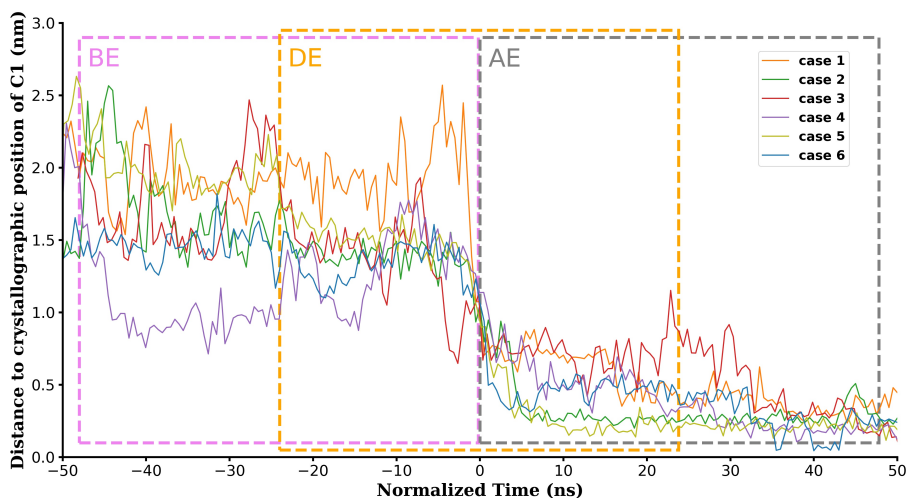


**FIGURE 4** The FA entering process occurs in a very narrow time window. Reaction coordinate of the C1 atoms of the fatty acids entering the protein (distance of the C1 atom of the fatty acids to their crystallographic position in 5CE4 structure). Time is normalized by choosing  $t = 0$  as the time in which the reaction coordinate has a value of 1 nm. BE, DE and AE stand for before entering, during entering and after entering, respectively. For this analysis, all the proteins were aligned with the 5CE4 structure.

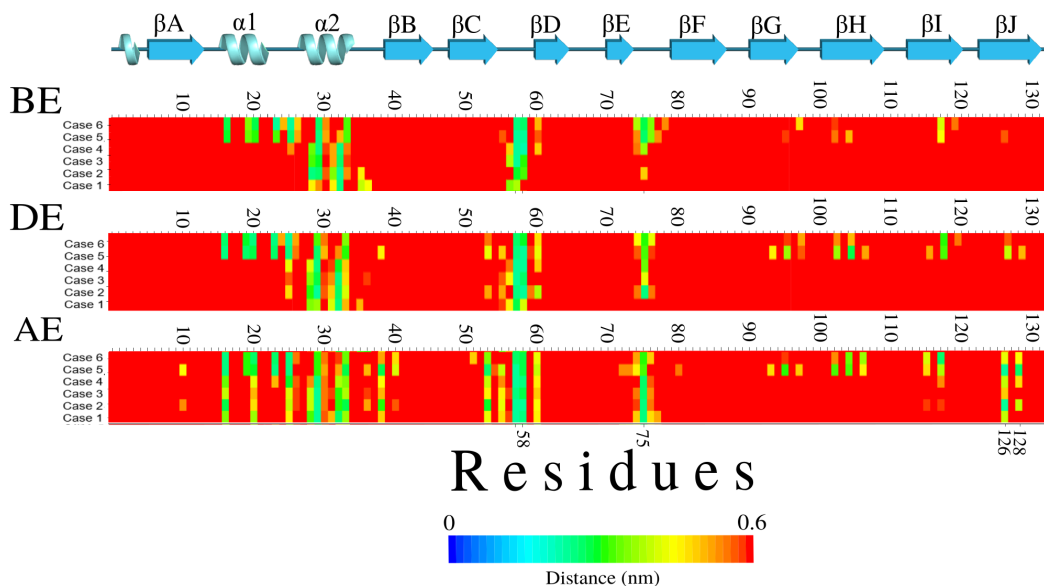


**FIGURE 5** The entrance of the FA into the h-FABP involves its interaction with  $\alpha 2$  helix,  $\beta C$ - $\beta D$  and  $\beta E$ - $\beta F$  loops. Contact map of the interactions between the fatty acid and all the protein residues for all the entrance cases studied BE, DE and AE stand for before entering, during entering and after entering, respectively, as in Figure 4.

cap is opened, nor the protein loses secondary structure. We can measure the portal opening of h-FABP from the distance between Val32 ( $\alpha 2$  helix) and Phe57 ( $\beta C$ - $\beta D$  loop) residues. We can see that the portal opening does not coincide with the entrance of the FA in any of the 6 cases (see Supp. Fig. ??). In this graph, we also observe, from the position of Val32 and Phe57 with respect to the COM of the protein, that the portal opening is mainly due to the movement of the  $\beta C$ - $\beta D$  loop, given the restriction imposed on the crystal to the movement of the  $\alpha 2$  helix. We can also note that the movement of Phe57 occurs mostly after FA entry, so we can associate it to a greater extent with the FA tail accommodation process. This last observation can be reinforced from the control plot, in which practically no movement of Phe57 is observed, and the FA tail position coincides with its crystallographic one.

The secondary structure is virtually not altered either, as can be seen, both by means of the algorithm Define Secondary Structure of Proteins (DSSP - Figure S5) [34] and helicity measures (Figure S6). The only case in which we detect a subtle and transient loss of secondary structure of  $\alpha 2$  helix is in case 6, where an oleic acid is entering the protein by its tail.

When analyzing the B-factors for the individual proteins (*i.e.*, Cases 1 to 6), it can be observed (see Figure S3-B) that the most perturbed residues compared to the control system, are Lys58 from  $\beta C$ - $\beta D$  loop, and Ala75 from  $\beta E$ - $\beta F$  loop, the same residues that show interaction with the FA.

## 4 | DISCUSSION

The main representation of how the portal region opens involves the loss of interaction between the  $\alpha 2$  helix and the  $\beta C$ - $\beta D$  loop, and between the  $\alpha 1$ - $\alpha 2$  and  $\beta E$ - $\beta F$  loops [35, 36], exposing the cavity [37]. However, the process of entry or exit of a single lipid has not been observed experimentally, and the structures obtained, both in the crystalline state and in solution, can not show intermediate states that can be unequivocally associated with a necessary step of the entry or exit of the ligand [35, 36, 38].

Seeking to restrict the degrees of freedom of the protein, NMR relaxation dispersion and H-D exchange in human intestinal FABP (I-FABP) studies have been carried out [12, 13], which in one case had their helical cap blocked by a disulfide bond with the  $\beta$  barrel and, in the other, had the inter- $\beta$ -sheet distance blocked by a disulfide bridge between residues 60 and 70. Even with these restrictions, studies show that ligand entry into the protein cavity is still possible with a partial local unfolding of  $\alpha 2$  helix.

Our experimental results show evidence of FA exchange in a crystalline environment where the helix-turn-helix cap is involved in the crystalline packing, and therefore its movement is strongly restricted. On the other hand, our computational results show no evidence supporting the necessity of an open conformation for FA entry, in which neither  $\alpha 1$  nor  $\alpha 2$  helices move away from the  $\beta$  barrel, thus exposing the protein cavity. In the cases where we detected an open conformation of the portal, this opening corresponds to a shift in the position of the  $\beta C$ - $\beta D$  loop (see Supplemental Figure ??) instead of the movement of the cap region. Anyway, there were some cases (cases 2, 4 and 5) in which there were two FAs struggling to enter the cavity and the entry of one of them occurred also without opening the portal. Likewise, in none of the six cases in which the entry of the FAs was evidenced did we observe a notorious local denaturation of the  $\alpha 2$  helix (see Supplemental Figure S6).

We can briefly describe the general behavior of the fatty acid as approaching the protein to interact initially by its hydrophobic tail with  $\alpha 2$  helix. In cases 1 to 4, once in this place, the FA head interacts forming a hydrogen bond with Lys58, and then, in most cases forms another hydrogen bond with the backbone of Ala75, giving place to the FA entrance. As we mentioned, for cases 5 and 6, the entrance starts with the tail exploring the protein cavity (besides not being in the final position). These two cases involve different ligands (palmitic and oleic acid, respectively) and

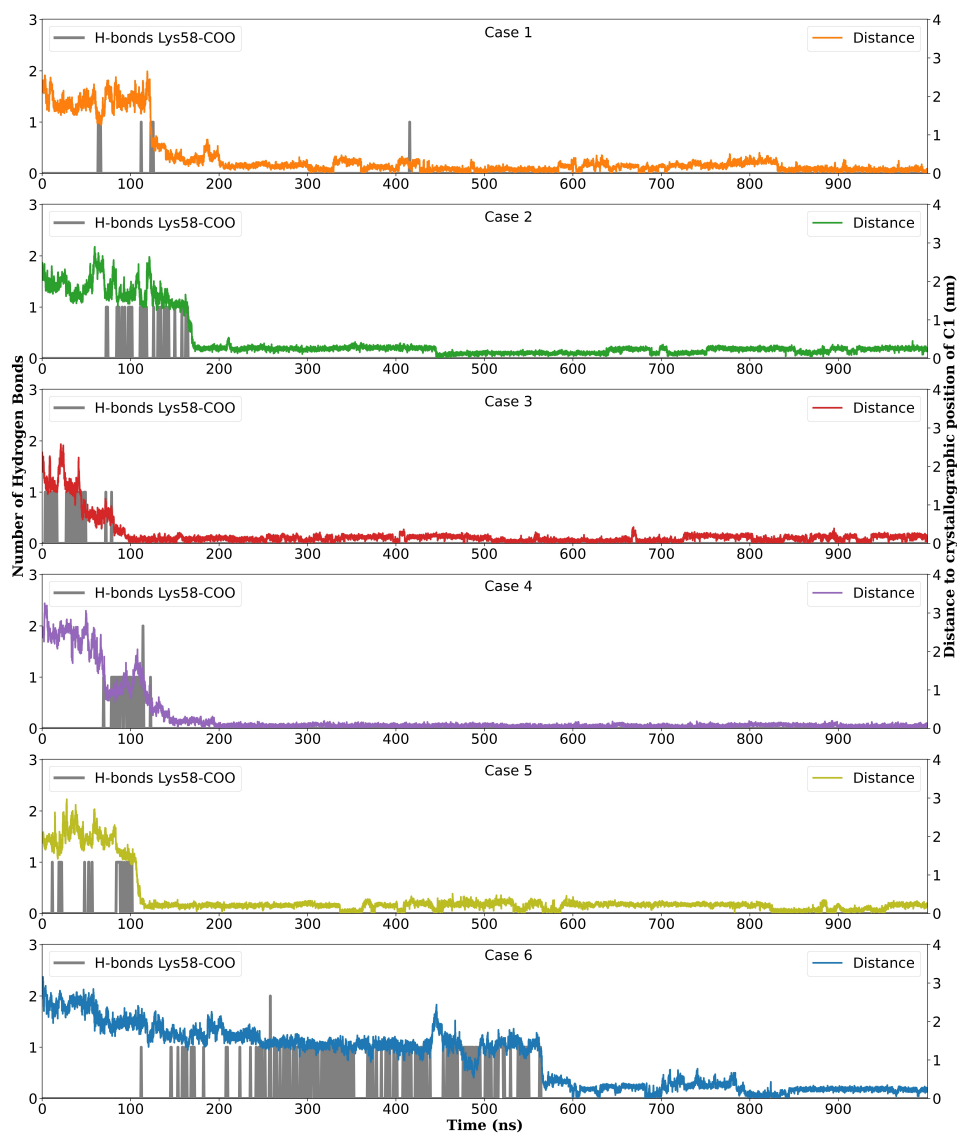


**FIGURE 6** The FA head interacts forming hydrogen bonds with Lys58 before entering into the cavity. Hydrogen bond count between Lys58 (grey) and the FA head (left axis) as a function of simulated time. On the right axis, we show the distance between the position of the C1 atom from the carboxylic head of the FA and its position in the 5CE4 crystallographic structure once each individual protein was aligned with the latter structure. From this figure, we can conclude that the interaction between the FA and Lys58 is previous to the entrance. The criteria for hydrogen bond calculations were: a limit of  $30^\circ$  for the hydrogen-donor-acceptor angle and of  $3.5 \text{ \AA}$  for donor-acceptor distance.

their tails are positioned in different places of the cavity when the head turns (Normalized time = 0 in our references). Although polar head turning is very fast and reaches residues Arg126 and Tyr128 as in the other four cases, the total process for the lipid to end up nestled inside the protein is slower than the mechanism described above. Even cases 5 and 6 are rare events in our simulations compared to the classical view (cases 1 to 4), this way of entry could be important from a functional point of view because it allows lipid entry from a hydrophilic environment where the polar head would be exposed and would be the first to enter or, in the opposite manner, a hydrophobic environment where the nonpolar tail would be exposed and thus initiate the process. Further studies will be necessary to understand the relevance of these mechanisms.

## 5 | CONCLUSIONS

In this paper, we probed by an original experimental approach that the FA interchange process in FABPs is possible even in a confined environment, such as a protein crystal. Our MD simulations show at an atomic level many cases of the FA entrance process. For the first four cases analyzed, once the FA is near the entrance portal, we distinguished two different events: First, in the order of tens of nanoseconds, the rapid entry of the FA head until it reaches the base of the protein cavity, close to residues Arg126 and Tyr128, where it finally stabilizes. Second, in the order of hundreds of nanoseconds, or even microseconds, a slow event in which the hydrophobic tail settles in the interior of the cavity. It is principally this last event which introduces perturbations in the conformation of the portal regions. Cases 5 and 6 are different because they both start with the entrance of the FA tail into the protein cavity. Otherwise, once the FA head interacts with Lys58, all the processes follow a similar behavior.

Despite certain regularities, the path that the FA head follows in the cavity interior or the time it takes for the hydrophobic tail to settle varies from case to case. We have observed some conformational fluctuations in the protein during the entry processes, but we have not been able to establish a causal relationship or a temporal correlation that leads to the description of a single mechanism or path, but rather a landscape through which the FA gets into the cavity. Furthermore, we found particular preferences that may indicate different pathways in different environments, such as an environment rich in FAs like a membrane.

Our conclusions do not mean that the results observed and mechanisms proposed in previous works do not occur or do not contribute to the optimal performance of the protein in a particular physiological environment, but we have observed a diversity of ways and paths that allows us to approach the problem from a broader perspective.

## Acknowledgements

The authors thank especially André Mitschler for his valuable support and for the experience he shared in the lab work, which deeply influenced us. This work was supported by Consejo Nacional de Investigaciones Científicas y Técnicas (CONICET) PIP 11220210100884CO, Universidad Nacional de La Plata (UNLP) of Argentina, the French Infrastructure for Integrated Structural Biology (FRISBI) ANR-10-INSB-005 and Instruct-ERIC. The crystallographic experiments were performed on the X06DA beamline at the Swiss Light Source, Paul Scherrer Institut, Villigen, Switzerland. We thank the "Nodo de Cálculo de la Universidad Nacional de Tierra del Fuego" (COFECYT 2018-240-APN-MCT) for the facilities to perform part of the calculations here presented. H.A.A. is a teaching researcher from UNLP. The CONICET supported Y.R.E.. C.M.C. is a member of CONICET - Argentina. E.I.H. is also a member of CONICET and a teaching researcher from UTN-F.R. Tierra del Fuego.

## Conflict of interest

The authors declare no conflicts of interest.

## references

- [1] Smathers RL, Petersen DR. The human fatty acid-binding protein family: Evolutionary divergences and functions. *Human Genomics* 2011;5(3):170.
- [2] Chmurzyńska A. The multigene family of fatty acid-binding proteins (FABPs): Function, structure and polymorphism. *Journal of Applied Genetics* 2006 Mar;47(1):39–48.
- [3] Storch J, Thumser AEA. The fatty acid transport function of fatty acid-binding proteins. *Biochimica et Biophysica Acta (BBA) - Molecular and Cell Biology of Lipids* 2000 Jun;1486(1):28–44.
- [4] Zimmerman AW, Veerkamp JH. New insights into the structure and function of fatty acid-binding proteins. *Cellular and Molecular Life Sciences (CMLS)* 2002 Jul;59(7):1096–1116.
- [5] Furuhashi M, Hotamisligil GS. Fatty acid-binding proteins: role in metabolic diseases and potential as drug targets. *Nature Reviews Drug Discovery* 2008 Jun;7(6):489–503.
- [6] Li HL, Wu X, Xu A, Hoo RLC. A-FABP in Metabolic Diseases and the Therapeutic Implications: An Update. *International Journal of Molecular Sciences* 2021 Aug;22(17):9386.
- [7] Rodríguez-Calvo R, Girona J, Alegret JM, Bosquet A, Ibarretxe D, Masana L. Role of the fatty acid-binding protein 4 in heart failure and cardiovascular disease. *Journal of Endocrinology* 2017 Jun;233(3):R173–R184.
- [8] Kozłowska D, Myśliwiec H, Harasim-Symbor E, Milewska AJ, Chabowski A, Flisiak I. Serum fatty acid binding protein 5 (FABP5) as a potential biomarker of inflammation in psoriasis. *Molecular Biology Reports* 2021 May;48(5):4421–4429.
- [9] Long D, Mu Y, Yang D. Molecular Dynamics Simulation of Ligand Dissociation from Liver Fatty Acid Binding Protein. *PLoS ONE* 2009 Jun;4(6):e6081.
- [10] Levin LBA, Ganoth A, Amram S, Nachliel E, Gutman M, Tsfadia Y. Insight into the interaction sites between fatty acid binding proteins and their ligands. *Journal of Molecular Modeling* 2009 Oct;16(5):929–938.
- [11] Guo Y, Duan M, Yang M. The Observation of Ligand-Binding-Relevant Open States of Fatty Acid Binding Protein by Molecular Dynamics Simulations and a Markov State Model. *International Journal of Molecular Sciences* 2019 Jul;20(14):3476.
- [12] Xiao T, Fan Js, Zhou H, Lin Q, Yang D. Local unfolding of fatty acid binding protein to allow ligand entry for binding. *Angewandte Chemie International Edition* 2016;55(24):6869–6872.
- [13] Xiao T, Lu Y, Fan Js, Yang D. Ligand entry into fatty acid binding protein via local unfolding instead of gap widening. *Biophysical journal* 2020;118(2):396–402.
- [14] Espinosa YR, Alvarez HA, Howard EI, Carlevaro CM. Molecular dynamics simulation of the heart type fatty acid binding protein in a crystal environment. *Journal of Biomolecular Structure and Dynamics* 2021;39(10):3459–3468.
- [15] Peeters R, Veerkamp J, Geurts van Kessel A, Kanda T, Ono T. Cloning of the cDNA encoding human skeletal-muscle fatty-acid-binding protein, its peptide sequence and chromosomal localization. *Biochemical Journal* 1991;276(1):203–207.
- [16] Zanotti G, Scapin G, Spadon P, Veerkamp J, Sacchettini J. Three-dimensional structure of recombinant human muscle fatty acid-binding protein. *Journal of Biological Chemistry* 1992;267(26):18541–18550.

- [17] Matsuoka S, Sugiyama S, Matsuoka D, Hirose M, Lethu S, Ano H, et al. Water-Mediated Recognition of Simple Alkyl Chains by Heart-Type Fatty-Acid-Binding Protein. *Angewandte Chemie International Edition* 2015;54(5):1508–1511.
- [18] Young AC, Scapin G, Kromminga A, Patel SB, Veerkamp JH, Sacchettini JC. Structural studies on human muscle fatty acid binding protein at 1.4 Å resolution: binding interactions with three C18 fatty acids. *Structure* 1994 Jun;2(6):523–534.
- [19] Howard EI, Guillot B, Blakeley MP, Haertlein M, Moulin M, Mitschler A, et al. High-resolution neutron and X-ray diffraction room-temperature studies of an H-FABP–oleic acid complex: study of the internal water cluster and ligand binding by a transferred multipolar electron-density distribution. *IUCr* 2016 Jan;3(2):115–126.
- [20] Otwinowski Z, Minor W. [20] Processing of X-ray diffraction data collected in oscillation mode. In: *Methods in Enzymology* Elsevier; 1997.p. 307–326.
- [21] DeLano WL, Bromberg S. *PyMOL user's guide*. DeLano Scientific LLC, San Carlos, California, USA 2004;.
- [22] Abascal JLF, Vega C. A general purpose model for the condensed phases of water: TIP4P/2005. *The Journal of Chemical Physics* 2005 Dec;123(23):234505.
- [23] Chen B, Potoff JJ, Siepmann JI. Monte Carlo Calculations for Alcohols and Their Mixtures with Alkanes. Transferable Potentials for Phase Equilibria. 5. United-Atom Description of Primary, Secondary, and Tertiary Alcohols. *The Journal of Physical Chemistry B* 2001 Mar;105(15):3093–3104.
- [24] Klinov A, Anashkin I. Diffusion in Binary Aqueous Solutions of Alcohols by Molecular Simulation. *Processes* 2019;7(12).
- [25] Olsson MH, Søndergaard CR, Rostkowski M, Jensen JH. PROPKA3: Consistent treatment of internal and surface residues in empirical pKa predictions. *Journal of Chemical Theory and Computation* 2011;7(2):525–537.
- [26] Hornak V, Abel R, Okur A, Strockbine B, Roitberg A, Simmerling C. Comparison of multiple Amber force fields and development of improved protein backbone parameters. *Proteins: Structure, Function, and Bioinformatics* 2006 Nov;65(3):712–725.
- [27] Wang J, Wolf RM, Caldwell JW, Kollman PA, Case DA. Development and testing of a general amber force field. *Journal of Computational Chemistry* 2004;25(9):1157–1174.
- [28] da Silva AWS, Vranken WF. ACPYPE - AnteChamber PYthon Parser interfacE. *BMC Research Notes* 2012 Jul;5(1).
- [29] Abraham MJ, Murtola T, Schulz R, Páll S, Smith JC, Hess B, et al. GROMACS: High performance molecular simulations through multi-level parallelism from laptops to supercomputers. *SoftwareX* 2015;1:19–25.
- [30] Bussi G, Donadio D, Parrinello M. Canonical sampling through velocity rescaling. *The Journal of Chemical Physics* 2007 Jan;126(1):014101.
- [31] Parrinello M, Rahman A. Polymorphic transitions in single crystals: A new molecular dynamics method. *Journal of Applied Physics* 1981 Dec;52(12):7182–7190.
- [32] Hess B, Bekker H, Berendsen HJ, Fraaije JGEM. LINCS: A linear constraint solver for molecular simulations. *Journal of Computational Chemistry* 1997;18(12):1463–1472.
- [33] Abraham MJ, Gready JE. Optimization of parameters for molecular dynamics simulation using smooth particle-mesh Ewald in GROMACS 4.5. *Journal of Computational Chemistry* 2011;32(9):2031–2040.
- [34] Kabsch W, Sander C. Dictionary of protein secondary structure: pattern recognition of hydrogen-bonded and geometrical features. *Biopolymers: Original Research on Biomolecules* 1983;22(12):2577–2637.
- [35] Sacchettini JC, Gordon JI, Banaszak LJ. Crystal structure of rat intestinal fatty-acid-binding protein: Refinement and analysis of the Escherichia coli-derived protein with bound palmitate. *Journal of molecular biology* 1989;208(2):327–339.

- 
- [36] Storch J, Thumser AE. The fatty acid transport function of fatty acid-binding proteins. *Biochimica et Biophysica Acta (BBA)-Molecular and Cell Biology of Lipids* 2000;1486(1):28–44.
- [37] Antúnez-Argüelles E, Robles-Gómez E. New insights in the opening mechanism of the heart-type fatty acid binding protein in its apo form (apo-FABP3). *Structural Chemistry* 2020;31(2):619–629.
- [38] Lücke C, Rademacher M, Zimmerman AW, Van Moerkerk HT, Veerkamp JH, Rüterjans H. Spin-system heterogeneities indicate a selected-fit mechanism in fatty acid binding to heart-type fatty acid-binding protein (H-FABP). *Biochemical Journal* 2001;354(2):259–266.

## Supporting Information

### Supplementary Videos

- Supplemental Video 1:  
Example of fatty acid entry into FABP in a crystalline environment. [LINK1](#)
- Supplemental Video 2:  
Construction of simulation box from PDB structure 5CE4. [LINK2](#)
- Supplemental Video 3:  
Representation of the path followed by the carboxylic carbon of the head of the fatty acid into the FABP protein interior. [LINK3](#)
- Supplemental Video 4:  
Six entrance cases of fatty acids into the FABP protein interior observed in our MD simulations. [LINK4](#)
- Supplemental Video 5:  
Comparison of the two cases in which we observed the FA entrance to the protein by their tail, showing the instant in which the FA heads turn inside the cavity to reach their final positions. Note that during the video the FA tails are not yet settled in their final position. [LINK5](#)

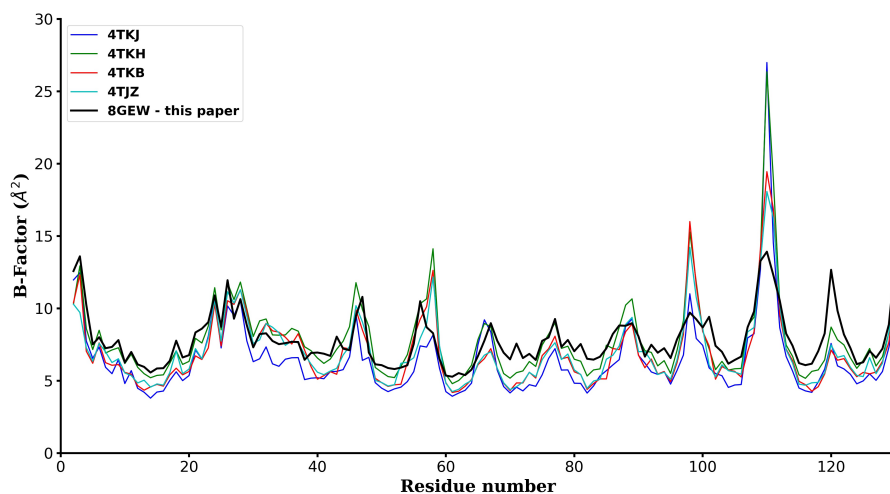


**FIGURE S1** Temperature Factors (B-Factors) for the structure after soaking in Br-palmitic solution (PDB 8GEW), compared to the corresponding B-Factors for structures from reference [17].

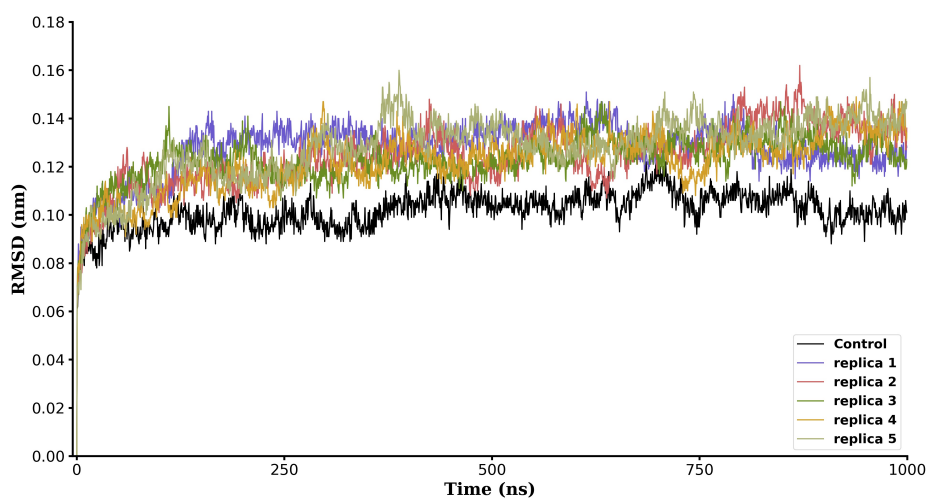


**FIGURE S2** Root mean Square Displacement (RMSD) of the atomic positions of the backbone for the five simulation replicas and for the control crystal.

**TABLE S1** Data Collection and Refinement Statistics of the crystal soaked with Br-Palmitic acid. Values in parentheses are for the highest-resolution shell.

Data collection	PDB entry: 8GEW
X-ray source, beamline	SLS, X06DA
Wavelength (Å)	0.729
Temperature (K)	100
Space group (one complex per a.u.)	P2 <sub>1</sub> 2 <sub>1</sub> 2 <sub>1</sub>
Unit-cell parameters (Å)	a=33.73 b=54.97 c=70.71
Resolution range (Å)	50 - 0.97 (1.0 - 0.97)
No. of observations	486292
Multiplicity	6.3 (5.9)
Completeness (%)	99.4 (98.4)
$R_{sym}$ (%)	6.9 (80.5)
Mean $I/\sigma(I)$	22.7 (2.07)
Refinement	
Refinement resolution range (Å)	30.47 - 0.97
$R_{work}$ (%)	0.13612
$R_{free}$ (%)	0.15314
No. of reflections for refinement	73632
Model used for MR	5CE4
$RMSD_{bonds}$ (Å)	0.013
$RMSD_{angles}$ (°)	1.894
Protein Atoms	2465
Water molecules	235
Ramachandran plot Favoured (%)	99.23
Ramachandran plot Accepted (%)	0.77
Ramachandran plot Outliers (%)	0

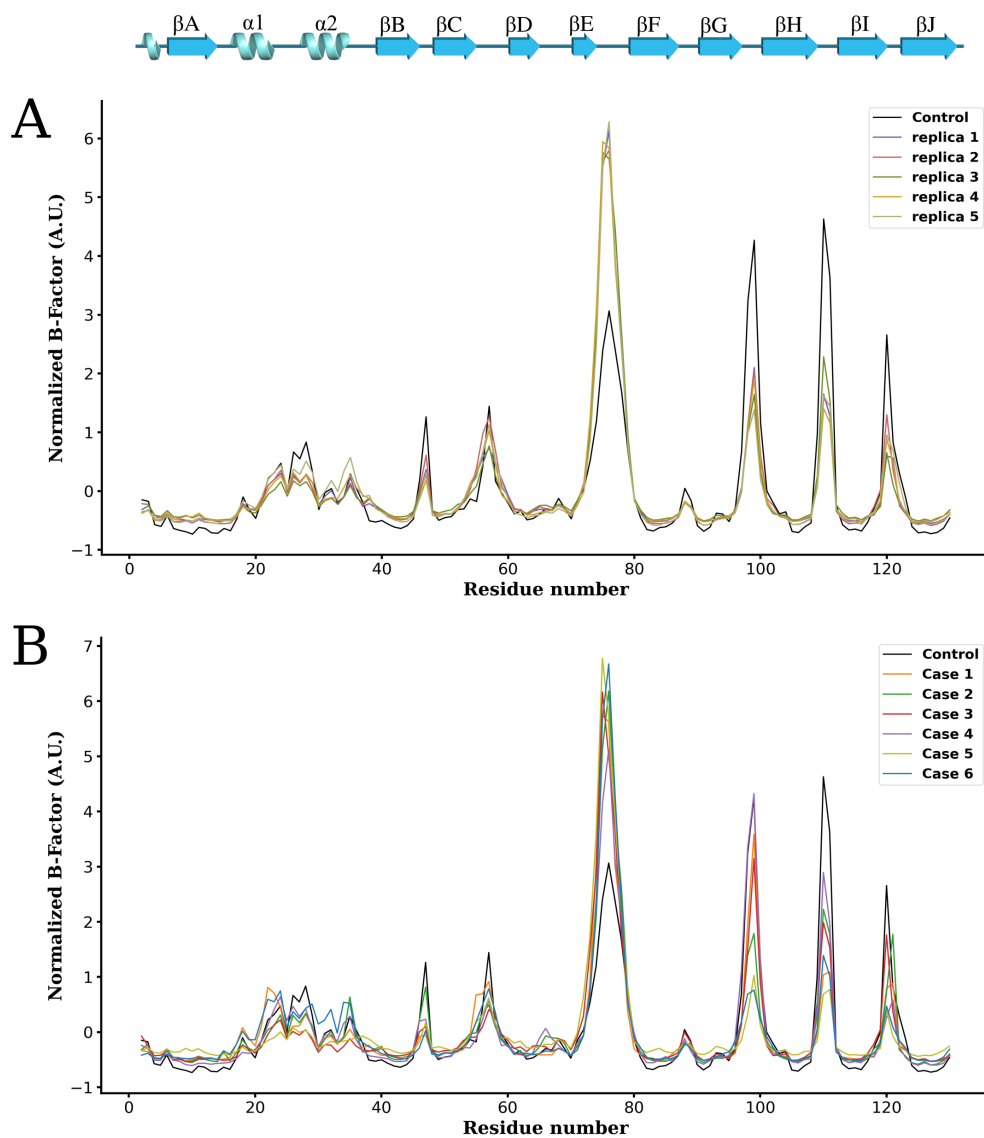


**FIGURE S3** A.- Temperature Factors (B-Factors) obtained by averaging the eight RMSF curves computed on the  $C\alpha$  atoms of each individual crystal proteins: Control and Replicas 1 to 5. B.- B-Factors of individual proteins for cases 1 to 6 compared with the control crystal (more stable structure with fatty acids in the protein cavity). All B-Factors were calculated for the  $C\alpha$  of amino acids 2 to 130.

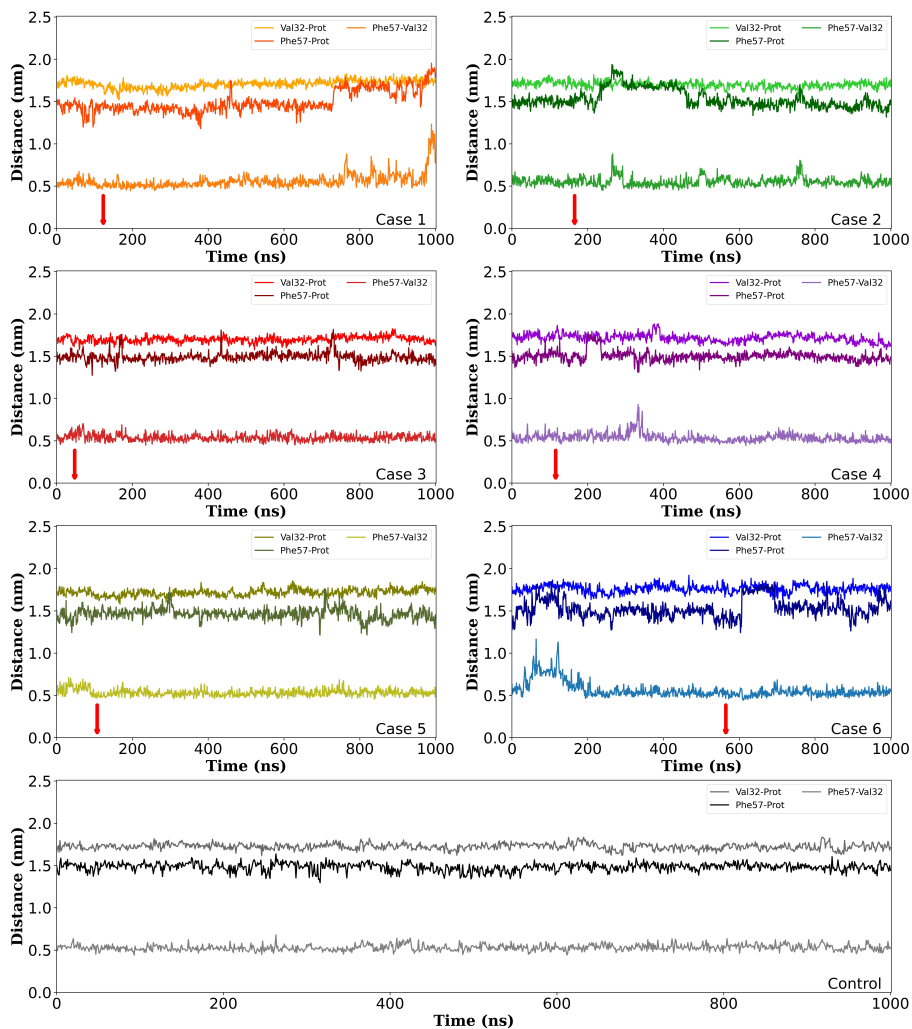


**FIGURE S4** Temporal evolution of the distance between amino acids Val32 and Phe57 of h-FABP and the center of mass of the protein in the cases 1 to 6 and also in one of the proteins of the control crystal. The distance between amino acids Val32 and Phe57 is also plotted as a measure of the portal opening.

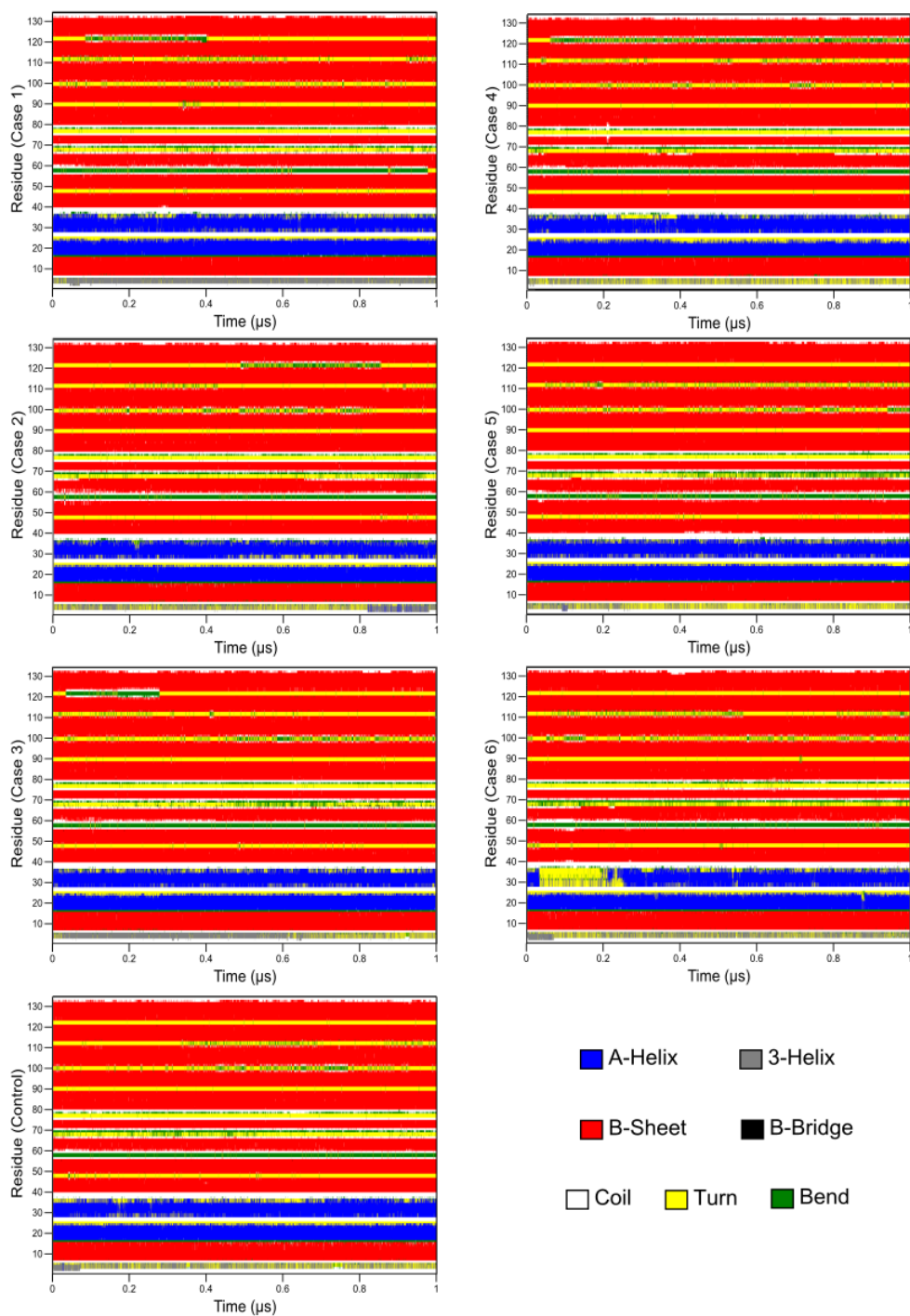


**FIGURE S5** Time evolution of the secondary structural elements of h-FABP (DSSP classification) in the cases 1 to 6 and also one of the proteins in the control crystal.

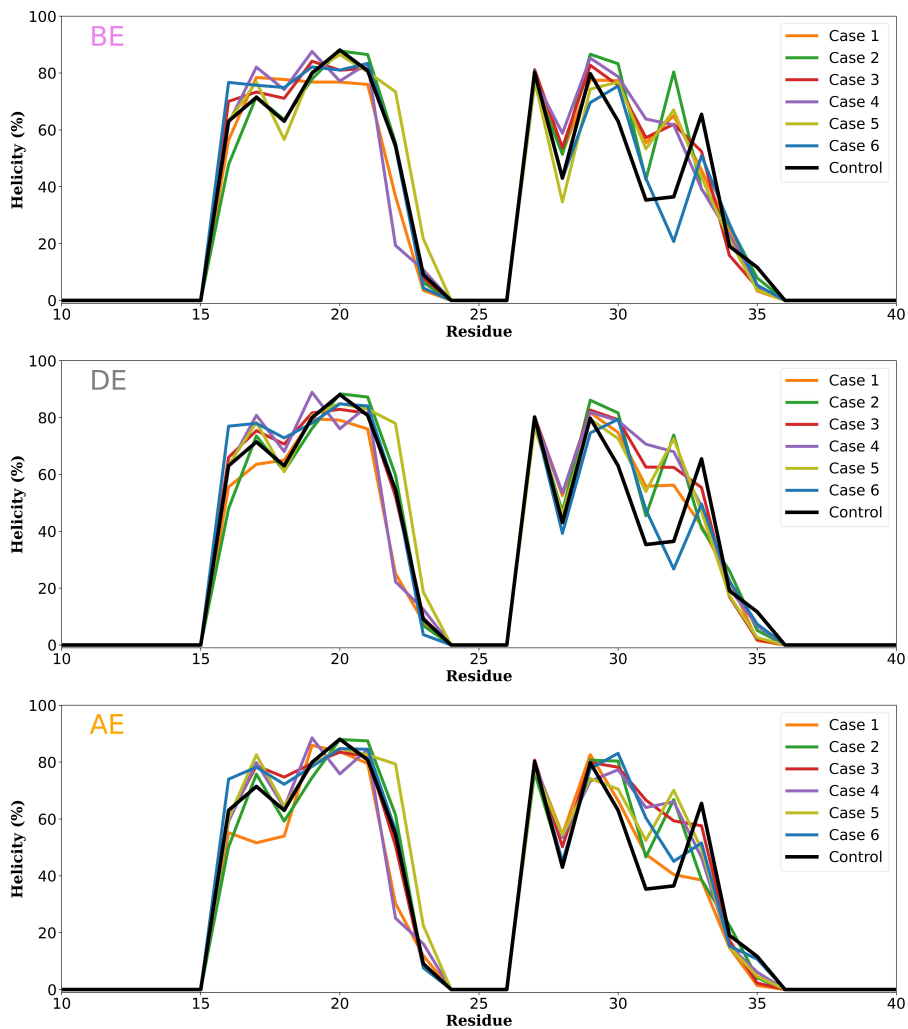


**FIGURE S6** Temporal percentage of the helicity for each residue on  $\alpha 1$  and  $\alpha 2$  helix of h-FABP, cases 1 to 6. BE, DE and AE stand for before entering, during entering and after entering, respectively. We show the percentage of helicity for the control simulation in an arbitrary time window of the same size for comparison purposes.